Title

The IgM receptor FcμR limits tonic BCR signaling by regulating expression of the IgM BCR

Journal

Nature Immunology, 18(3)

ISSN

1529-2908

Authors

Nguyen, Trang TT

Kläsener, Kathrin

Zürn, Christa

et al.

Publication Date

2017-03-01

DOI

10.1038/ni.3677

Peer reviewed

HHS Public Access

Author manuscript

Nat Immunol. Author manuscript; available in PMC 2017 July 30.

Published in final edited form as:

Nat Immunol. 2017 March ; 18(3): 321–333. doi:10.1038/ni.3677.

The FcμR Limits Tonic BCR Signaling by Regulating IgM-BCR Expression

Trang T. T. Nguyen[1,2], **Kathrin Kläsener**[3,4,5], **Christa Zürn**[5], **Patricia A. Castillo**[2,6], **Ingrid Brust-Mascher**[7], **Denise M. Imai**[8], **Charles L. Bevins**[2,6], **Colin Reardon**[7], **Michael Reth**[3,4,5], and **Nicole Baumgarth**[1,2,8,9]

[1]Center for Comparative Medicine, University of California, Davis, Davis, California, USA

[2]Graduate Group in Immunology, University of California, Davis, Davis, California, USA

[3]BIOSS Centre for Biological Signalling Studies, University of Freiburg, D-79104 Freiburg, Germany

[4]Department of Molecular Immunology, Institute of Biology III at the Faculty of Biology of the University of Freiburg, Freiburg, Germany

[5]D-79104, and at the Max Planck Institute of Immunobiology and Epigenetics, D-79108 Freiburg, Germany

[6]Dept. Medical Microbiology & Immunology, University of California, Davis, California, USA

[7]Dept. Anatomy, Physiology & Cell Biology, University of California, Davis, California, USA

[8]Comparative Pathology Laboratory, School of Veterinary Medicine, University of California, Davis, California, USA

[9]Dept. Pathology, Microbiology & Immunology, University of California, Davis, Davis, California, USA

Abstract

The IgM Fc receptor (FcμR), originally cloned as “Fas-apoptosis inhibitory molecule (FAIM3/TOSO)” can function as a cell surface receptor for secreted IgM on a variety of cell types. We report that FcμR also is expressed in the trans-Golgi network of developing B cells, where it constrains IgM- but not IgD-BCR transport. In FcμR absence, IgM-BCR surface expression was increased, resulting in enhanced tonic BCR signaling. B cell-specific FcμR-deficiency enhanced spontaneous differentiation of B-1 cells, resulting in increases in natural IgM levels, and

Correspondence should be addressed to: Nicole Baumgarth, DVM, PhD, Center for Comparative Medicine, University of California, Davis, County Rd 98 & Hutchison Drive, Davis, CA 95616, nbaumgarth@ucdavis.edu, phone: 530 – 754 5813, FAX: 530 – 752 7913.

Author contributions

T.T.T.N. and N.B. designed experiments, analyzed data and wrote the manuscripts. C.L.B., K.K. and M.R. provided help with experimental design. T.T.T.N., K.K., C.Z., and P.A.C., performed experiments. I.B.M and C.R helped with STED and confocal microscopy and image analysis. D.M.I performed pathological evaluation of *Fcmr*$^{flx/flx}$*Cd19*-Cre mice. All authors provided edits to the manuscript.

Competing Financial Interests

The authors declare that no conflict of interest exists.

dysregulated B-2 cell homeostasis, causing spontaneous germinal center formation, increased serum autoantibody titers, and excessive B cell accumulation. Thus, FcμR/FAIM3 is a critical regulator of B cell biology by constraining IgM-BCR transport and cell surface expression.

Introduction

The Fc-receptor for IgM (FcμR) is a transmembrane receptor that was initially named Fas apoptosis inhibitory molecule 3 (FAIM3 or TOSO), because transfection experiments indicated this protein protected Jurkat T cells from Fas-induced programmed cell death *in vitro*[1, 2, 3]. More recently, however, several studies identified FAIM3 as the long elusive Fc-receptor for IgM that is expressed on the cell surface of human and mouse primary follicular B cells. Those studies failed to find evidence for a Fas-inhibitory activity on these cells[4, 5]. They therefore renamed the molecule “FcμR”. Others since confirmed the IgM-binding activity of this receptor[6, 7, 8].

FcμR surface expression was reported for various leukocyte populations, including granulocytes, macrophages, monocytes, dendritic cells, and regulatory T cells. The highest expressions were noted in B cells[8, 9, 10]. Studies with global FcμR-deficient mice suggested that the receptor broadly regulates cellular activation, such as inflammatory responses of dendritic cells and regulatory T cells in autoimmune diseases[10], the maturation and differentiation of dendritic cells in lymphocytic choriomeningitis virus infection[11], and the production of reactive oxygen species of neutrophils[9]. Global FcμR-deficient mice also showed increases in serum IgG autoantibody titers, as well as increased concentrations of natural serum IgM[6, 7]. The mechanism by which FcμR regulates B cell homeostasis and autoantibody production has not been elucidated.

Recent confocal imaging suggested that the FcμR might also interact with the membrane-bound IgM (mIgM)-BCR on the B cell surface, where these molecules co-localize[12]. The mIgM-BCR consists of mIgM and associated signaling chains CD79a and CD79b. IgM undergoes extensive posttranslational modifications and is sorted in the trans-Golgi network (TGN) for transport to the cell surface[13]. The BCR provides constitutive, low-levels “tonic” signals, required for B cell survival[14]. During bone marrow (BM) development, mIgM-BCR signaling regulates B cell selection. Once B cells are mature, antigen encounter by the BCR induces B cell activation and differentiation[15].

In humans, dysregulated expression of the FcμR has been associated with various B cell malignancies[16, 17]. On CLL cells and transiently transfected HeLa cells the FcμR internalized soluble IgM and transported it from the cell surface to the lysosome for degradation, suggesting it may uptake IgM-antigen complexes. In transfected HeLa cells localization of the FcμR was detected not only on the cell surface and following internalization in the lysosomes, but also in the trans-Golgi network (TGN)[16]. Thus indicating that mIgM-FcμR interaction could occur in the TGN also during development of B cells.

Indeed, using high resolution microscopy and proximal ligation assays we demonstrate that the FcμR interacts directly with mIgM in the TGN of immature B cells and that this

interaction regulates BCR surface expression and thereby tonic BCR signaling. The lack of FcμR-mediated suppression of BCR-surface expression, and therefore signaling, in B cells of tissue-specific FcμR-deficient mice (*Fcmr* $^{flx/flx}$*Cd19*-Cre), resulted in dysregulated spontaneous activation and differentiation of B-1 and B-2 cells and development of a lymphoproliferative disorder. Our data support a model whereby the FcμR constrains BCR expression to regulate fundamental B cell homeostasis and biology.

RESULTS

FcμR surface expression is highest on B cells

Consistent with prior reports[4, 7, 8, 18], the highest surface expression of the FcμR was seen on B cells, but mostly absent on CD4 and CD8 T cells (Supplementary Fig. 1a,b). Myeloid cell populations, such as Gr-1$^+$ (granulocytes), CD11b$^+$/F4/80$^+$ (macrophages) and CD11c$^+$ (dendritic cells) showed low surface expressions (Supplementary Fig. 1a,b). mRNA expression analysis confirmed *Fcmr* expression by all peripheral B cell subsets. It was highest in splenic follicular (FO) B cells (CD19$^+$IgD^{hi}CD23$^+$) and splenic B-1 cells (CD19^{hi}IgM^{hi}IgD^{lo}CD23$^-$CD43$^+$), and somewhat lower in marginal zone (MZ) B cells (CD19$^+$CD21^{hi}CD23$^-$) and in peritoneal cavity B-1 cells (Fig. 1a). Protein expression analysis confirmed high surface expression by splenic B-1 cells but also by MZ B cells. Surface expression of the FcμR appeared low in the peritoneal cavity (Figure. 1b and Supplementary Fig. 1c). Splenic FO B cells showed higher FcμR expression compared to FO B cells in inguinal lymph nodes (Figure. 1b and Supplementary Fig. 1c). Thus, the FcμR is dynamically regulated in various B cell subsets and by tissue location.

During BM development, FcμR expression was seen first at the late pre-B cell stage, with rapidly increasing expression among immature B cells (Fig. 1c,d and Supplementary Fig. 1d). Confocal microscopy confirmed expression of the FcμR on the surface of B220$^+$CD43$^-$IgM$^{lo/+}$IgD$^-$ immature B cells (Fig. 1e). But we also noted an unexpected strong intracellular presence of the FcμR. Two-color confocal microscopy of primary immature B cells localized the FcμR to the trans-Golgi network (TGN), using the marker TGN-38 (Fig. 1e). The TGN plays a central role in post-translational modifications and the sorting of mIgM for transport[13, 19]. This suggested that the FcμR may interact with mIgM during B cell development, when IgM is modified and first transported to the cell surface. Together, the data demonstrate correlated expression of the FcμR and mIgM during the transition from the late pre-B to the immature B cell stage. In developing B cells the FcμR receptor is present in two distinct compartments that include the cell membrane and the TGN.

The FcμR interacts with secreted and membrane IgM

To study the direct effects of IgM-FcμR interaction in B cells, we created B cell-specific *Fcmr*$^{-/-}$ mice using the Cre-lox system, with Cre expression driven by the *Cd19* promoter. For most experiments the *Fcmr* $^{flx/flx}$*Cd19*-Cre+ mice were compared to littermate *Fcmr* $^{flx/flx}$*Cd19*-Cre$^-$ controls. Flow cytometry (Supplementary Fig. 1a) and gene expression analysis (Fig. 1f) on flow cytometry-sorted splenic B cells confirmed the B cell-specific deletion of the *Fcmr*.

Despite expression of the FcμR early in B cell development, *Fcmr*$^{flx/flx}$*Cd19*-Cre+ mice showed no overt defects in B cell development. All B cell developmental stages were present at frequencies and numbers comparable to their controls (Supplementary Fig. 2a). Furthermore, there was no difference in the rate at which the receptor-deficient mice accumulated immature CD93^{+} B cells in the spleen 12 days after sublethal irradiation (Supplementary Fig. 2b,c).

As we and others showed previously[4, 16, 20], secreted IgM (sIgM) can bind to the cell surface of B cells. As expected, genetic ablation of the FcμR reduced sIgM binding to B cells *in vitro (*Fig. 2a and Supplementary Fig. 3a), which we tested by exposing purified spleen B cells from controls and *Fcmr*$^{flx/flx}$*Cd19*-Cre^{+} mice to purified and biotinylated sIgM. Surface sIgM binding was rapidly lost, independent of the B cell source (Supplementary Fig. 3a,b), suggesting rapid internalization. T cells did not bind to sIgM (Supplementary 3b). To determine whether similar binding of sIgM to B cells occurs *in vivo,* and if so, what effects removal of the FcμR may have on that binding, we adoptively transferred control or *Fcmr*$^{flx/flx}$*Cd19*-Cre+ IgH^{b}-expressing B cells into congenic IgH^{a}-expressing mice. 72 h after transfer the amount of secreted IgM (IgM^{a}) binding to the surface of wild-type and *Fcmr*$^{-/-}$ B cells was compared by flow cytometry, identifying the transferred cells via IgD^{b} (Fig. 2b). The CD19^{+}IgD^{b} Fcmr$^{-/-}$ B cells bound significantly less sIgM^{a} compared to B cells from controls, as indicated by reduced MFI for IgM^{a} staining (Fig. 2b–c), *In vivo* bound sIgM was lost as rapidly in culture as after incubation with sIgM *in vivo* (Supplementary Fig. 3c). In contrast, and unexpectedly, the *Fcmr*$^{-/-}$ B cells stained more strongly for the mIgM-BCR (IgH^{b}) compared to their controls (Fig. 2c–d). Thus, the FcμR facilitates the *in vivo* binding of natural IgM to the surface of B cells and appears to be involved also in IgM-BCR surface expression.

Immunoprecipitation studies demonstrated that the FcμR can directly bind to and interact with IgM[4, 12]. To distinguish FcμR interaction with the membrane and secreted form of IgM, respectively, we first conducted stimulated emission depletion (STED) microscopy, which provides resolution of two proteins down to 50nm in living cells[21]. To differentiate between mIgM and sIgM we isolated B cells from mixed BM irradiation chimeras, which were generated by adaptive transfer of BM from wild-type (IgH^{b}) and $\mu_s^{-/-}$ (IgH^{a}) mice into lethally irradiated recipients. B cells from $\mu_s^{-/-}$ mice lack the μ_s exon, encoding the secreted form of IgM, but they express mIgM[22]. In these chimeras, all sIgM is therefore derived from the IgH^{b} expressing wild-type B cells. Staining for IgD with allotype-specific mAb determined the Ig-genotype of follicular (FO) B cells, such that analysis of IgD^{a}-expressing $\mu_s^{-/-}$ cells distinguished mIgM (IgM^{a}) expression from sIgM (IgM^{b}) –binding directly *ex vivo*. The exquisite specificity of the monoclonal antibodies anti-IgM^{a} (DS.1) and anti-IgM^{b} (AF6.78.25) is well known[23, 24, 25] and was further demonstrated by us (Supplementary Fig. 4a–c). Analysis of FO B cells revealed that mIgM^{a} was expressed evenly on the cell surface, whereas sIgM^{b} was more focally spaced (Fig. 2e). Secreted- but not mIgM was also seen in vesicles directly beneath the cell membrane (Fig. 2e,f), consistent with the previously reported internalization of sIgM into endosomes[16]. Direct *ex-vivo* visualization of sIgM-internalization by splenic FO B cells suggested that this is an ongoing process. FO B cells lacked measurable mIgM in intracellular compartments (Fig. 2e,f), likely due to low turnover rates of mIgM[26].

Next we used three-color confocal microscopy on FO B cells from the same mice to study co-localization of the FcμR with mIgM and/or sIgM. On the cell membrane the FcμR co-localized with both, mIgM and sIgM (Fig. 2f, arrows indicate co-localization), while there was little if any co-localization in the TGN, (Supplementary Fig. 5a). In contrast, STED microscopy of immature B cells showed that the FcμR co-localized with IgM both on the cell membrane as well as in the TGN (Fig. 2g,h and Supplementary Fig. 5b). The intracellular co-localization was strongly focal/vesicular, with individual vesicles containing both FcμR and IgM in close proximity to the cell membrane, suggesting transport (Supplementary Fig. 5b).

To provide further evidence of FcμR and mIgM interaction, we used the Fab-based Proximity Ligation Assay (Fab-PLA) with a 10–20 nm resolution capacity[27]. Strong Fab-PLA signals (depicted in red), indicative of protein-protein interaction, were detected in the cytosol of saponin-treated $B220^{+}CD43^{-}CD25^{-}IgD^{-}$ immature BM B cells at a subcellular region that stained with the Golgi-marker lectin-GSII-Alexa 488 (Fig. 2i-top and Supplementary Fig. 5c). The FcμR-mIgM interaction occurred also on the cell surface (stained for GM-1 with the cholera toxin subunit B-FITC) of intact immature B cells, albeit to a lesser extent (Fig. 2i-bottom). In contrast, the splenic mature FO B cells displayed only weak FcμR-mIgM interactions and only on the cell surface (Fig. 2j-compare top to bottom and Supplementary Fig. 5c). Together the studies revealed strong interactions of the FcμR with IgM in the TGN of immature B cells, and much weaker interactions on the cell surface of mature B cells.

FcμR-mIgM interaction constrains BCR surface expression

The TGN of primary B cells contains mIgM but not sIgM[16, 19], thus the FcμR could affect mIgM transport. Flow cytometry on B cells from *Fcmr*$^{flx/flx}$*Cd19*-Cre and wild type mice showed similar staining for total surface IgM (Fig. 3a). However, separate staining for sIgM-binding and mIgM expression after transfer of either control or *Fcmr*$^{flx/flx}$*Cd19*-Cre B cells (IgH^{b}) to (IgH^{a}) mice, revealed that increased expression of mIgM by the *Fcmr*$^{-/-}$ B cells was offset by reduced surface binding of sIgM, masking differences in IgM-BCR expression. This was confirmed by the transfer of FO B cells from either *Fcmr*$^{flx/flx}$*Cd19*-Cre or control mice into B cell-deficient mice. While staining for total (secreted plus membrane-bound) IgM was similar prior to transfer (Fig. 3a), 72h after transfer increased surface IgM staining was seen on B cells from *Fcmr*$^{flx/flx}$*Cd19*-Cre mice compared to controls, presumably because the bound sIgM was internalized, leaving only surface mIgM (Fig. 3b). Consistent with this, Igα (CD79a) expression was significantly increased in the *Fcmr*–deficient B cells compared to controls (Fig. 3c). Increased mIgM expression by *Fcmr*–deficient B cells was not due to alterations in gene transcription (Fig. 3d). The data suggested that the interaction with the FcμR in the TGN of developing immature B cells constrains the transport of mIgM, and/or its retention on the cell surface.

To provide evidence of FcμR-mediated mIgM transport regulation, we expressed chimeric GFP-μm (IgM) heavy chains (HC) either alone, or as chimeric IgM-BCR together with the signaling subunits CD79a and CD79b (Fig. 3e) in a S2 Drosophila cell system[28]. As expected, only a fully assembled IgM-BCR was placed on the cell surface and its amount

was significantly reduced after co-expression of the FcμR (Fig. 3f,g). IgD-BCR expression was not altered, when co-expressed with the FcμR either in different or in the same cell (Fig. 3f,g). To determine whether FcμR affects IgM-BCR transport, we measured the re-appearance of IgM-BCR GFP-fluorescence after photobleaching (FRAP) on the surface of transfected S2 cells (Fig. 3h,i). The mobile fraction (Mf) and the half-time recovery data showed that the reappearance of IgM-BCR fluorescence, was significantly reduced in the presence of the FcμR, while IgD-BCR expression was not affected. (Fig. 3h,i). We conclude that the FcμR directly and specifically restricts transport of the IgM-BCR to the surface of developing B cells.

Enhanced tonic BCR signaling in *Fcmr*$^{-/-}$ B cells

Surface BCR expression is required for B cell survival, and the amount of surface BCR influences both B cell development and mature B cell reactivity. Therefore, we determined next whether increased mIgM-BCR surface expressions by *Fcmr*$^{-/-}$ B cells affected steady state or “tonic” BCR signaling. Tonic BCR signaling triggers phosphorylation of phosphoinositide 3-kinase (PI3K) and its down-stream targets, including Erk, Ras and Akt[29, 30]. The transcriptional repressor Foxo1 is a major target of phosphorylated Akt (pAkt, Ser473) in tonic BCR signaling[29]. De-repression of the Foxo1 target *Cdkn1b* can lead to cell cycle entry of FO B cells[29, 31]. Foxo1 also controls cell survival, in part via repression of the cellular stress sensor and pro-apoptotic gene *Bcl2l11*[29, 32].

Expression of the regulatory (p85) as well as the catalytic (p110) subunit[33] of PI3K were significantly increased in B cells from *Fcmr*$^{flx/flx}$*Cd19*-Cre mice compared to controls (Fig. 4a,b), as was pAkt in purified B-2 and in B-1 cells (Fig. 4c,d). B-1 cells expressed more pAkt compared to B-2 cells in control and *Fcmr*$^{flx/flx}$*Cd19*-Cre mice (Fig. 4d). Heightened tonic BCR signaling of B-1 cells is consistent with their increased auto-reactive repertoire[34, 35]. Phosphorylated Btk (pBtk) was also increased in freshly isolated *Fcmr*$^{-/-}$ B-1 and B-2 cells (Fig. 4e,f) and increased pAkt and pBtk were seen in *Fcmr*$^{-/-}$ B cells derived from chimeras established with BM from global *Fcmr*$^{-/-}$ compared to control chimeras (Supplementary Fig. 6a,b). Cre-toxicity was not responsible for phosphorylation differences, as increased PI3K/pAkt were only observed in *Fcmr*$^{flx/flx}$*Cd19*-Cre mice and not in *Fcmr*$^{wt/flx}$*Cd19*-Cre, *Fcmr*$^{wt/flx}$*Cd19*-Cre^{-} mice, or *Fcmr*$^{flx/flx}$*Cd19*-Cre^{-} mice (Supplementary Fig. 7a,b). A good correlation existed between the expressions of pAkt and pBtk expressed by B cells and surface expressions of IgM (Fig. 4g and data not shown). This correlation was stronger in B cells from *Fcmr*$^{flx/flx}$*Cd19*-Cre mice than in controls, presumably because IgM staining is labeling the BCR only, while in wild-type B cells it labels both mIgM and sIgM; the latter not likely affecting BCR signaling. The data suggest that the stronger signaling in *Fcmr*$^{-/-}$ B cells is the direct outcome of enhanced mIgM expression.

Assessment of mRNA expression of three Foxo1 target genes showed expected changes in *Fcmr*$^{flx/flx}$*Cd19*-Cre B cells compared to controls, all indicative of enhanced tonic BCR signaling. The cell cycle inhibitor *Cdkn1b* (*P27*) and the pro-apoptotic *Bcl-2* family member *Bcl2l11* were significantly reduced in the absence of FcμR, while *Aicda*, a gene upregulated by Foxo1 activation was significantly increased (Fig. 4h). *Rag1* was not expressed in B cells

from either control or *Fcmr*$^{flx/flx}$*Cd19*-Cre mice (Fig. 4h). The data indicate that the FcμR regulates tonic BCR signaling by constraining surface expression of mIgM during B cell development.

To determine whether the absence of the FcμR affected B cell response to BCR crosslinking, we compared the responses of purified FO B cells from control and *Fcmr*$^{flx/flx}$*Cd19*-Cre mice to anti-IgM stimulation. Both, pAkt expression and B cell proliferation were comparable in these cultures (Fig. 4i–j). However, consistent with the ex *vivo* results, the *Fcmr*$^{-/-}$ B cells expressed more pAkt in the absence of stimulation after culture, compared to control B cells (Fig. 4j). Consistent with the reduced expression of the pro-apoptotic regulator *Bcl2l11*, *in vitro* cultures of *Fcmr*$^{-/-}$ B-1 and B-2 cells showed increased cell survival (Fig. 4k,l). This survival advantage was lost after stimulation with anti-IgM, anti-IgM plus anti-Fas, and lipopolysaccharide (Fig. 4k,l). Thus, the absence of the FcμR and resulting increases in BCR expression, enhanced tonic BCR signaling and B cell survival, while not significantly affecting signaling after strong anti-IgM mediated BCR cross-linking.

FcμR regulates natural IgM and autoantibody production

Increased BCR expression and resulting increases in tonic BCR signaling are expected to affect B cell homeostasis. Indeed, serum sIgM concentrations in *Fcmr*$^{flx/flx}$*Cd19*-Cre mice were twice that of their controls (Fig. 5a), similar to those reported for global *Fcmr*$^{-/-}$ mice[6, 7], while IgA concentrations were comparable and IgG concentrations were consistently, but not significantly, increased (Fig. 5b,c). Explaining the increases in serum IgM concentrations, frequencies of IgM secreting cells in spleen and BM were also greatly increased in *Fcmr*$^{flx/flx}$*Cd19*-Cre mice (Fig. 5d). In addition, IgM spot sizes appeared bigger than those of controls (Fig. 5d). Frequencies of spontaneous IgG secreting cells were also increased (Fig. 5e), and anti-dsDNA IgM and IgG titers were significantly elevated (Fig. 5f,g) in *Fcmr*$^{flx/flx}$*Cd19*-Cre mice, as seen also in global *Fcmr*$^{-/-}$ mice[7, 8]. However, after normalization of autoantibody concentrations to total Ig concentrations, the relative amounts of IgM anti-dsDNA were reduced rather then enhanced (Fig. 5f), while the relative amounts of anti-dsDNA IgG remained elevated (Fig. 5g). Together, the data demonstrate that direct FcμR signaling suppresses the development of natural IgM and of IgG autoantibody-producing cells in a B cell-intrinsic manner.

The FcμR was shown to inhibit Fas–FasL-mediated apoptosis in transfected T cell lines[3]. We found that Fas-induced cell death *in vitro* was only measurable in cultures of *Fcmr*$^{-/-}$ B-1 and FO B cells, but not in controls. This apparent inhibitory effect of the FcμR on Fas-mediated killing directly correlated with higher frequencies and absolute numbers of Fas-expressing CD38^{low}PNA^{+} germinal center B cells in the spleens of *Fcmr*$^{flx/flx}$*Cd19*-Cre mice (Fig. 5h,i). Importantly, the observed increases in tonic BCR signaling seem to lead to increased spontaneous B cell activation and germinal center formation, a likely source of the increased auto-reactive serum IgG titers (Fig. 5g). The apparent protection from Fas-induced cell death in the presence of the FcμR observable *in vitro* thus appears to be due mainly to the suppression of spontaneous B cell activation and therefore reduced Fas-expression. This

is further supported by the fact that Fas-induced cell death *in vitro* only reduced the frequencies of *Fcmr*$^{-/-}$ B cell survival to frequencies seen in control B cell cultures.

Natural IgM is important for early immune protection against bacteria and viruses such as influenza[24, 36, 37]. Consistent with elevated baseline concentrations of total serum IgM, concentrations of natural IgM that binds influenza A/Puerto Rico 8/34 (A/PR8) were significantly elevated in infection-naïve *Fcmr*$^{flx/flx}$*Cd19*-Cre mice compared to controls. The increased natural IgM levels before (Fig. 5j), and at day 1 after infection with A/PR8 (Fig. 5k,l), correlated with increased early control of lung influenza viral loads (Fig. 5m). We conclude that the FcμR expression in B cells reduces protective natural IgM serum levels, but also controls potentially harmful auto-reactive IgG.

Enhanced B-1 activation in *Fcmr* $^{flx/flx}$*Cd19*-Cre mice

Increased BCR signaling leads to enhanced B-1 cell development, a cell population largely responsible for natural IgM production[35]. As expected from the increased serum IgM concentrations, *Fcmr*$^{flx/flx}$*Cd19*-Cre mice showed strong increases in the frequencies and numbers of splenic B-1 cells, particularly CD5^{+} B-1a cells (Fig. 6a and Supplementary Fig. 7c), while their relative and absolute numbers in the peritoneal cavity were normal (Fig. 6b, Supplementary Fig. 7d). BM B-1 cell numbers were also higher, although this did not reach statistical significance (Fig. 6c). Controls, including *Fcmr*$^{flx/flx}$*Cd19*-Cre-, *Fcmr*$^{wt/flx}$*Cd19*-Cre- and *Fcmr*$^{wt/flx}$*Cd19*-Cre+ had B-1 cell populations similar to those of wild-type mice (Supplementary Fig. 7c). We conclude that the FcμR regulates B-1 cell activation and natural IgM secretion by regulating BCR-expression.

To determine whether *Fcmr*$^{-/-}$ B-1 cells are responsible for the increased IgM production in *Fcmr*$^{flx/flx}$*Cd19*-Cre mice, we generated neonatal Ig-allotype chimeras, in which only B-1 cells (IgH^{b}) lacked expression of the *Fcmr*$^{-/-}$, while all BM-derived B cells were wild-type (IgH^{a}). Control chimeras were reconstituted with *Fcmr*$^{flx/flx}$*Cd19*-Cre^{-} peritoneal cavity cells (IgH^{b}). Frequencies of *Fcmr*$^{-/-}$ B-1 cells (IgM^{b}) in the peritoneal cavity were comparable to chimeras generated with control B-1 cells, but were at least double that in spleen and BM (Fig. 6d). Moreover, *Fcmr*$^{-/-}$ B-1 cells developed about twice as many CD138^{+} plasma cells compared to control B-1 cells (Fig. 6e), and the frequencies of B-1 cell-derived IgM^{b} secreting cells were significantly increased (Fig. 6d), while as expected, frequencies of IgM secreting B-2 cells (IgM^{a} – thus wild-type) were comparable (Fig. 6f, right). The frequencies of IgM secreting B-1 cells (IgM^{b}) were more than 2-fold higher in *Fcmr*$^{-/-}$ B-1 chimeras compared to controls, as measured by ELISPOT (Fig. 6f, left). Consequently, serum IgM levels generated from *Fcmr*$^{-/-}$ B-1 cells (IgM^{b}) were substantially increased (Fig. 6g).

Analysis of chimeras generated by reconstituting lethally irradiated B cell deficient (μMT) mice with peritoneal lavage cells from *Fcmr*$^{flx/flx}$*Cd19*-Cre (IgH^{b}), or controls (IgH^{b}), as a source of B-1 cells, and BM cells from wild-type (IgH^{a}) mice as a source of B-2 cells, yielded comparable results (Supplementary Figs. 8–9). We conclude that increased BCR signaling in *Fcmr*$^{-/-}$ B-1 cells directly controls natural IgM production by enhancing their differentiation to IgM-secreting cells in spleen and BM, likely following stimulation by auto-antigens.

B-2 cell lymphocytosis in *Fcmr* $^{flx/flx}$*Cd19*-Cre mice

Increased IgG autoantibody production in *Fcmr* $^{flx/flx}$*Cd19*-Cre mice suggested that direct FcμR signaling also regulates the BM-derived B cell compartments. Marginal zone (MZ) B cells are negatively regulated by strong BCR signaling[38]. Consistent with findings in one global *Fcmr*$^{-/-}$ mouse line[6, 7, 20], but not another[8], we found significant reductions in relative frequencies of splenic MZ B cells in *Fcmr* $^{flx/flx}$*Cd19*-Cre mice compared to controls, while the relative frequencies of the FO B cell compartment appeared largely unaffected (Fig. 7a). However, taking total numbers of splenocytes into account, total MZ B cell pools were actually normal, while the numbers of splenic FO B cells were increased in these mice (Fig. 7a).

We also noted significant increased cell cycling and cell survival in *Fcmr* $^{flx/flx}$*Cd19*-Cre mice, specifically increased frequencies of cycling, Ki67^{+} FO B cells and total numbers of dividing B-1 and B-2 cells, as measured by BrDU incorporation (Fig. 7b–c). *Fcmr* $^{flx/flx}$*Cd19*-Cre mice also yielded fewer 7AAD^{+}, dead and dying B-1 and B-2 cells (Fig. 7d). The data explain that already by 3 months of age *Fcmr* $^{flx/flx}$*Cd19*-Cre mice showed significant increases in spleen cellularity and spleen enlargement (Fig. 7e,f) and by 8 months pronounced splenomegaly with expanded follicular compartments, as assessed histologically (Fig. 7g).

Discussion

This study reveals a new function for the FAIM3/FcμR in B cells, namely the control of surface mIgM-BCR expression and thereby the regulation of tonic BCR signaling. The identified extensive interaction of the FcμR with mIgM in the TGN of developing B cells and its inhibitory effect on mIgM accumulation on the cell surface, suggests that the FcμR exerts its control by regulating the transport of mIgM. The FcμR is thus identified as a critical regulator of B cell homeostasis.

The reported dysregulated expression of the FcμR in various human B cell malignancies further underscores its importance in shaping the balance between constraining and overshooting B cell responses to self and foreign antigens, as well as for support of B cell survival and rapid clonal expansion in response to pathogens. The lymphoproliferative disorder that develops in *Fcmr* $^{flx/flx}$*Cd19*-Cre mice over time is reminiscent of human cases of leukemic mantle cell lymphoma, diffuse large B cell lymphoma, follicular lymphoma, marginal zone lymphoma, and Hodgkin’s lymphoma, where a lack of FcμR expression was reported[16]. Intriguingly, the FcμR is overexpressed in other lymphomas, for example chronic lymphocytic leukemia, a malignancy of IgM^{+} B cells. The up-regulation of the FcμR could be an attempt by the cells to constrain chronic B cell activation and B cell expansion in these patients. Although we did not observe malignant B cell transformation in mice, this may be due to the relatively short lifespan of mice compared to humans. Worth noting, there have been no previous reports of lymphoproliferative disorders in the three global FcμR knockout mouse strains generated by others[1, 7, 8]. Further work is required to determine whether expression of the FcμR on cells other than B cells may also indirectly affect B cell activation.

The FcμR-mediated control of BCR expression and signaling limits the protective capacity of B-1 cells by reducing natural IgM concentrations. Increased production of natural IgM was reported previously in global *Fcmr*$^{-/-}$ mice[6, 7]. Our studies demonstrated the B cell-intrinsic nature of this regulation and identify fully differentiated CD138^{+} splenic B-1 cells as source of this increased protective IgM. Thus, while FcμR-mediated reduced tonic IgM-BCR signaling limits B cell activation and autoantibody production by B-2 cells[7, 8], it also constrains the protective capacity of B-1 cells.

Both, $\mu_s^{-/-}$ and *Fcmr*$^{-/-}$ mice generate autoantibodies[20, 39], which could indicate that sIgM-FcμR interactions regulate autoantibody production. The underlying mechanisms of autoantibody-production in these two genetically altered mice, however, appear distinct. $\mu_s^{-/-}$ show extensive alterations in B cell development, starting as early as at the pro/pre-B transition[20], before significant FcμR expression and change the repertoire of the developing B-1 and B-2 cells. These changes result in increased pools of anergic and auto-antibody producing B-2 cells, an increased MZ B cell compartment and a near complete loss of peritoneal, but not splenic B-1 cells[20]. In contrast, B cell development appears unaffected in *Fcmr*$^{flx/flx}$*Cd19*-Cre mice, and the B-2 cell repertoire showed no major differences in immunoglobulin heavy-chain variable region (IGVH) usage (unpublished observations). In further contrast to the $\mu_s^{-/-}$ mice, *Fcmr*$^{flx/flx}$*Cd19*-Cre mice had increased B cell pools with reduced, not increased, frequencies of MZ B cell, as well as expanded, rather than reduced B-1 cell pools. Thus, the impact on B cell homeostasis differs greatly between mice lacking sIgM and FcμR. This supports our conclusion that the regulation of B cell development by the FcμR is due mainly to its intracellular interactions with mIgM and thus control of BCR expression, rather than its interaction with sIgM on the B cell surface. Our data suggest a plausible scenario, in which mildly auto-reactive peripheral B cells that have escaped tolerance-induction in *Fcmr*$^{flx/flx}$*Cd19*-Cre mice experience chronically-enhanced tonic BCR-signaling via auto-antibody binding and/or by enhanced BCR auto-aggregation, due to enhanced IgM-BCR expression. This may result in the development of spontaneous auto-antigen induced germinal centers, class-switch recombination and an increased production of IgG autoantibodies.

While enhanced B cell responsiveness in the *Fcmr*$^{flx/flx}$*Cd19*-Cre mice caused spontaneous germinal center formation and autoantibody production, exposure to influenza virus induced germinal centers of normal size and following normal kinetics of induction and involution (unpublished observations). Differential regulation of self- and foreign antigen-induced germinal centers is seen also in other autoimmune disease mouse models[40, 41]. B cells from *Fcmr*$^{flx/flx}$*Cd19*-Cre mice show spontaneous activation, despite normal expression of IgD-BCR. Recent studies by Jumaa and colleagues[42] suggested that the IgM-BCR is superior in responding to monovalent antigens, whereas the IgD-BCR requires polyvalent antigens. The data could suggest that tonic BCR-signaling is induced mainly by IgM-BCR mediated binding to monovalent antigens, while stimulation by highly multivalent foreign antigens/pathogens effectively activates IgD-BCR, which is unaffected by FcμR-deficiency.

While this study focuses on FcμR-mIgM interaction in the TGN, by generating mixed BM irradiation chimeras between $\mu_s^{-/-}$ and allotype-mismatched wild type mice, we distinguished the interaction of the FcμR with mIgM and sIgM *ex vivo* for the first time. The

data provide a striking image of B cells continuously uptake of sIgM, which then accumulates in endosomal compartments[16]. Given the self-reactive repertoire of natural IgM, this uptake may result in the continued presentation of self-antigens to T cells and could help with an ongoing tolerization of the T cell compartment[43]. In support, spontaneous germinal centers develop in the *Fcmr* $^{flx/flx}$ *Cd19*-Cre mice, presumably requiring the breaking of tolerance in both, T cell as well as B cell compartments.

Methods

Mice

Male and female 8 – 12 week old C57BL/6 (IgH^b), B6.Cg-Igh^a Thy1^a Gpi1$^{a/}$J (IgH^a), and B cell-deficient μMT mice were obtained from The Jackson Laboratories. *Fcmr*$^{flx/flx}$ mice were generated by the UC Davis Mouse Biology Program MBP) using ES cells with a targeted deletion of exon 4 of the *Fcmr*, generated by the UC Davis MBP (Gene identification, MGI: 1916419) (https://www.komp.org/geneinfo.php?geneid=57632). Mice were then bred with *Cd19*-Cre$^{+/-}$ mice to generate *Fcmr* $^{flx/flx}$ Cre$^+$ mice with a B cell-specific deletion of the *Fcmr* $^{flx/flx}$ Cre$^-$ littermates served as controls. All mice were kept in specific-pathogen-free housing, in HVAC-filtered filter-top cages and are monitored for the absence of 17 common mouse pathogens. Mice were euthanized by overexposure to carbon dioxide. The Animal Use and Care Committee of the University of California, Davis, approved all procedures and experiments involving animals.

Mixed BM chimeras were generated by adoptively transferring equal numbers sIgM-deficient (μ_s $^{-/-}$, IgH^a) and wild-type C57BL/6 (IgH^b) BM cells into two months old C57BL/6 mice, lethally irradiated by exposure to a gamma-irradiation source 24 h prior to transfer. Chimeras were rested for at least 7 weeks before analysis.

To generate neonatal B-1 cell chimeras newborn B6.Cg IgH^a mice were treated with anti-IgM^a antibodies (clone DS1.1) i.p. twice weekly for 6 weeks to temporarily deplete their B cells. Two δ three days after birth, pups were reconstituted with peritoneal lavage cells from either FcμR$^{flx/flx}$ Cre$^+$ or Cre$^-$ mice (IgH^b), as a source of *Fcmr*$^{-/-}$ or wild-type B-1 cells, respectively. Mice were analyzed no earlier than 2 months after end of anti-IgM^a treatment, at which point all B-2 cells are host-derived (IgH^a) and most B-1 cells are peritoneal cavity donor-derived (IgH^b)[25, 44, 45].

B cell isolation and *in vitro* B cells assays

The following B cell populations were negatively enriched by auto-MACS (Miltenyi Biotech) using depletion cocktails and anti-biotin Microbeads (Miltenyi Biotech) after Fc-blocking: Spleen B cells, biotinylated conjugates against CD90.2 (30-H12), F4/80 (BM8), Gr-1 (RB6-8C5), and NK1.1 (PK136). Peritoneal cavity B-1 cells, CD90.2, F4/80, Gr-1, NK1.1, and CD23 (B3B4). FO B cells were isolated via positive selection with anti-CD23-biotin. For proliferation assays, the cells were labeled with 0.5 μM CFSE as previously described[20]. Cells were cultured with anti-IgM (Goat anti-mouse IgM $(Fab)_2$ (Jackson ImmunoResearch) 20 μg/ml medium (RPMI/10%FCS/L-glutamine/streptomycin), anti-Fas IgG (BD Pharmingen, Jo2) 100 ng/ml medium, or LPS (Sigma) 20 μg/ml medium in 96-well

round-bottom plates for 72 h at 37°C in 5% CO_2. Flow cytometry analysis was done to identify the number of dividing cells (CFSE low) and frequencies of live cells ($7AAD^-$).

For *in vivo* stimulation of B-1 cells 1.5×10^6 peritoneal cavity cells from *Fcmr* $^{flx/flx}$ *Cd19*-Cre or Creδ control mice (IgH^b) were injected i.p into B6.Cg-IgH^a mice, followed by i.p injection of 20 μg LPS/mouse. The sera and spleens from mice were collected 1.5 days later to measure IgM secretion and IgM-secreting cells by ELISA.

ELISA and ELISPOT assays

DNA-specific IgM and IgG and total IgM, IgM^a, IgM^b, IgG concentrations in sera were measured as previously described[20, 46]. For detection of influenza A/Puerto Rico/8/34 binding IgM, ELISA plates were coated with 250 hemagglutinating units A/PR8[47]. Binding was revealed with goat anti-mouse IgM (Southern Biotech) as previously described[24]. IgMδ and IgG-secreting cells in the spleens and BMs were enumerated by ELISPOT[46].

Flow cytometry

Single-cell suspensions from spleen, BM, and peritoneal cavities were stained with anti-CD16/32 (2.4G2) 5 μg/ml for 20 min on ice to block Fc receptors. Cells were stained with antibody conjugates against FcμR-biotin (MBL; clone: 4B5; in-house conjugated with biotin); IgD^a-biotin (AMS-9.1), IgM^a-biotin (DS.1), CD5-biotin (53.7–8) (in-house generated), PNA-biotin (Vector Laboratories, B-1075) and the following fluorochome-conjugates: Streptavidin (SA)-Qdot 605 (Invitrogen), Fas-PE (eBioscience,15-A7), CD43-PE (S7), CD21-FITC (7G6), CD38-FITC (90), IgD-Cy7PE (11-26C), IgD^b-Cy7PE (AF6.122), IgM^b-(FITC, PE) (AF6-78.25), IgM-(APC, Cy7APC) (331), IgM^a-APC (DS.1), CD45R-(FITC, Cy7APC, Cy55APC) (RA3-6B2), CD19-(Cy5PE, APC) (ID3) (all in-house generated). Dead cells were excluded by live/dead-pacblue (Invitrogen) or $7AAD^+$ (BD Pharmingen) staining for 30 min. Staining for BrdU was done according to the manufacturer's protocols using a BD Pharmingen BrdU Flow Kit. Cell cycle analysis were done as previously described[20].

Phosphoflow: Cells were surface-stained before fixation (BD Cytofix) for 30 min on ice. Cells were washed and permeabilized with Perm/Wash buffer (BD) for 30 min on ice. Cells were washed and stained with anti-phospho-Akt-PE (BD phosphoflow, pS473) on ice for 30 mins. For phospho-Btk, fixed and permeabilized cells were stained with anti-phospho-Btk PE (Y551/Y511; eBioscience) at 22°C for 30 min. For PI3K-p110 subunit and Igα (CD79a) staining, fixed and permeabilized cells were stained with anti-p110 Alexa Fluor 488 (Abcam ab202666, clone EPR5515(2)), or anti-CD79a PE (eBioscience, HM47). For PI3K-p85 subunit staining, fixed and permeabilized cells were stained with anti-p85 (Abcam ab189403, 6G10), anti mouse IgG1-biotin (SouthernBiotech,1070-05), and with SA-Qdot 605 for 30 min at each step. Flow cytometry was performed using a Fortessa (BD) equipped with 4-lasers and optical set-up for up to 22 parameter analysis. Flow cytometry-sorting of spleen and BM B cell subsets was done using a flow cytometry Aria (BD Biosciences)[20].

Fluorescence Recovery After Photobleaching (FRAP)

Schneider S2 cells were transfected with BCR IgM-GFP or IgD-GFP chimeras with and without co-expression of FcμR and FRAP analyzed in Ringer solution at 22°C using a ZEISS LSM 780 laser scanning microscope. In brief, the pixel size was adjusted to 0.44 μm, the image size to 512 × 512 pixel, and the pixel time to 1.58 μs. Entire cells were bleached per region of interest (ROI) using the 488, 561, 633, and 405 nm lasers simultaneously. GFP was bleached until 10% of the initial intensity was reached (duration varied from 1–5s). In total, 171 image series containing about 12–15 ROI were recorded with the 488/514 nm Argon laser. Each image series included ten pre-bleach (every 5s) and 161 post bleach images (every 5–20s) in a 16-bit format. Images were taken until GFP recovery plateaued. Vertical drift was not observed during the measurement because S2 cells adhere to the plate. Values for background analysis were taken from non-bleached and bleached areas containing no cells. The obtained recovery traces (with time set to 0 for the first frame post bleach) were corrected for the photomultiplier (PMT) error, background and bleaching during recovery, and normalized to the pre-bleach fluorescence intensity defined as 100%. The mobile fraction (Mf) was calculated using the published equation[48, 49] and the photobleaching correction[50]:

$$\begin{aligned}\mathrm{Mf}=100*(\mathrm{F}_{\mathrm{precell}}-\mathrm{F}_{\mathrm{background}})/(\mathrm{F}_{\infty\mathrm{cell}}\\ -\mathrm{F}_{\mathrm{background}})*((\mathrm{F}_{\infty}\\ -\mathrm{F}_{\mathrm{background}})-(\mathrm{F}_{0}-\mathrm{F}_{\mathrm{background}}))/((\mathrm{F}_{\mathrm{pre}}\\ -\mathrm{F}_{\mathrm{background}})-(\mathrm{F}_{0}-\mathrm{F}_{\mathrm{background}})).\end{aligned}$$

Where $F_{precell}$ is the whole cell pre-bleach intensity, F_{pre} is the bleach ROI pre-bleach intensity, $F_{\infty cell}$ is the asymptote of fluorescence recovery of the whole cell, and $F_{background}$ is the mean background intensity that includes PMT correction. F_{∞} is the bleach ROI asymptote, and F_0 is the bleach ROI immediate post bleach intensity. Curve fitting and asymptote calculation was performed in GraphPad Prism (nonlinear regression analysis).

The half-time of recovery ($t_{1/2}$) was determined by solving the following equation[49]: $F_{(t)}=[F_0+F_\infty(t/t_{1/2})]/[(1+(t/t_{1/2})]$. Where F_0 is the bleach ROI immediate post bleach intensity, F_∞ is the asymptote of the bleach ROI fluorescence recovery, t is the time for each ROI intensity value in seconds, and $t_{1/2}$ is the time required for the bleach ROI to recover to 50% of the asymptote. For one experiment and condition 10 data sets with 9–12 cells of each transfection were analyzed, normalized, and averaged for M(f) as well as half-time recovery. In total, two independent FRAP experiments were performed.

In vitro sIgM-binding assay

The *in vitro* sIgM binding assay was performed as previously described[20]. Briefly, cells were incubated with sIgM-biotin (SouthernBiotech, Clone 11E10) for 30 minutes at 4°C. Binding was revealed by staining with Streptavidin-Qdot605.

In vitro assay of FcμR and membrane IgM interaction

FcμR cDNA was amplified and cloned into pBluescript from splenic B cells of C57BL/6 mice with primers *Fcmr*-29s (5′-AAGGCTCCCAGGTGATCGG-3′) and *Fcmr*-1491a (5′-GGGGTGAAAAATTAGCCTGTAATTG-3′). The restriction sites (EcoRI and SacI) were added using primers 5′-TGCATGCAGAATTCCCATGGACTTTTGGCT T-3′ and 5′-TGCATGCAGAGGTCACTCATTGGCATGAAGA-3′. *Fcmr* was inserted in pRmHa-3 plasmid at the EcoRI and SacI sites. FcμR construct was co-expressed with GFP-μmHc and mcherry-δmHc constructs in Drosophila S2 cells, as previously outlined[28] and stained with anti IgM-V450 (BD) or anti IgD-Alexa 647 (Abcam).

Proximity-Ligation Assay

Proximity-ligation assay (PLA) was performed as previously described[27]. In brief: PLA-probes against specific targets, the following unlabeled Abs were used: anti-IgM (BD Biosciences, 1B4B1), anti-FcμR (Novus Biologicals, pc). Fab fragments were prepared with Pierce Fab Micro preparation kit (Thermo Scientific) using immobilized papain according to the manufacturer's protocol. After desalting (Zeba spin desalting columns, Thermo Scientific), the Fab fragments were coupled with PLA Probemaker Plus or Minus oligonucleotides (Sigma-Aldrich) to generate Fab-PLA probes. Naive B cells were enriched by MACS depletion using anti-CD43 MicroBeads (Miltyeni Biotec) according to the manufacturer's protocol. BM B cells were negatively selected by auto-MACS (Milteny Biotech) using anti CD43-biotin, anti CD25-biotin, and anti IgD-biotin depletion and streptavidin Microbeads (Miltenyi Biotech) after Fc-blocking. The enriched B cells were rested overnight in complete RPMI 1640 medium. For in situ PLA, B cells were settled on polytetrafluoroethylene slides (Thermo Fisher Scientific) for 30 min at 37 °C. BCR. Fixation, permeabilization, and PLA reactions were conducted according to the previously mentioned protocol[27]. Surface costaining for GM-1 was performed with cholera-toxin suB-FITC (Sigma-Aldrich). Intracellular Golgi was stained with Golgiδ lectin GSII Alexa-488 (Molecular Probes) according to manufacturer's protocol. Resulting samples were directly mounted on slides with DAPI Fluoromount-G (SouthernBiotech) to visualize the PLA signals in relationship to the nuclei. Microscopic images were acquired with a Zeiss 780 Meta confocal microscope (Carl Zeiss). For each experiment a minimum of 250 immature B and 750 B-2 cells from several images were analyzed (ImageJ). Raw data were exported to Prism software (GraphPad Software). For each sample, the mean PLA signal count per cell was calculated from the corresponding images and the statistical significance with Student's t-test. Co-localization of confocal images (Pearson's correlation (total R) and Manders split coefficients) of TGN, 488 nm laser (channel1), and PLA, 561 nm laser (channel 2) were analyzed for 40 cells with FIJI (ImageJ).

Histology

Spleens were fixed in neutral buffered formalin, embedded in paraffin, sectioned (4μm thickness), and stained with H&E.

Immunofluorescence confocal microscopy

Splenic IgH^a IgM$^{-/-}$ B cells were negatively enriched from mixed IgM$^{-/-}$ and wild-type chimeras by auto-MACS (IgD^b, CD90.2, F4/80, Gr-1, NK1.1 biotin). After fixing with BD cytoperm/cytofix buffer, IgM$^{-/-}$ B cells were incubated with IgM^b biotin (clone AF6-78.25), IgM^a Alexa 488 (clone DS.1) followed by fluorescent SA Alexa 555 (Life Technologies; Ref. S21381) each for 30 min. For FcμR staining, the cells were stained with FcμR Abs (MBL, clone 4B5, IgG2a) and then with anti-rat IgG2a Alexa 647 (Abcam, clone 2A 8F4, Ref. ab172333). mIgM and sIgM were imaged with the same system in STED mode, depletion was accomplished with a 592nm laser for Alexa 488 and a 660nm laser for Alexa 555.

Late pre-B cells and immature B cells (CD45R$^+$CD43$^-$IgD$^-$) were sorted by flow cytometry from C57BL/6 BM cells, fixed with BD cytoperm/cytofix buffer and washed with Perm/Wash buffer (BD). Cells were stained with FcμR-biotin (MBL, clone 4B5) and trans-Golgi network antibody TGN38 (BD, Cat. 610898, 2/TGN38) at 22°C for 30 mins. After washing, fluorescent SA-Alexa 555 (Life Technologies; Ref. S21381) and IgM Alexa 488 (clone 331) were added and incubated for 30 min followed by anti-mouse IgG1 Alexa 647 (Biolegend, Cat. 406617) to visualize TGN-38. The cells were washed 3 times with PBS. Cells were transferred in 20 μl PBS to coverslips (Corning; Cat. 2850-22), and mounted with Prolong Diamond Antifade Mountant (Life Technologies, Ref. P36961). Images were acquired on a Leica SP8 TCS STED 3X microscope system with an HC PL APO 100X/1.4 NA STED objective either in confocal (IgM and TGN 38) or STED (FcμR) mode. Fluorophores were excited with a white light laser and a 660 nm depletion laser was used for STED imaging.

qRT-PCR

Total RNA from different B cell subsets was isolated with RNeasy (Qiagen) and stored at −80C in RNA storage buffer (Ambion) until use. Complementary DNA was prepared as previously described[20]. *Rag1*, *Aicda*, *Cdkn1b*, *Bcl2l11* and membrane IgM mRNA expression were measured as described previously[29, 51]. *Fcmr* expression was measured using a commercial primer/probe set (Mm01302388_m1; Applied Biosystems). Quantitative PCR was performed using a 7900HT Fas Real-Time PCR system (Applied Biosystems) with following cycles: 50°C for 2 min, 95°C for 10 min, and 40 cycles of 95°C for 15s and 60°C for 1 min. Relative expression was normalized to *Gapdh* (Mm.P.T.39a.1; IDT).

Influenza virus infection and viral load determination

Fcmr$^{flx/flx}$*Cd19*-Cre and control mice were anesthetized with isoflurane and infected intranasally with 20 PFU influenza A/Puerto Rico/8/34 (A/PR8; H1N1) per mouse in 40 μl PBS. Lungs were harvested 24 h after infection and RNA was extracted from lung homogenates (gentleMACS, Miltenyi Biotec) using a QIAamp Viral RNA mini kit (Qiagen). Viral and cDNA was prepared as described[20]. A/PR8 virus loads were measured using primer/probe sets for a conserved portion of the viral matrix protein AM151 (5′-CATGGAATGGCTAAAGACAAGACC-3′), AM397 (5′-AAGTGCACCAGCAGAATAACTGAG-3′), AM245 (5′-6FAMCTGCAGCGTAGACGCTTTGTCCAA AATGTAMRA-3′). Quantitative PCR

was performed using Standard TaqMan Cycling conditions as described above. 10-fold serial dilution of cDNA from stock A/PR8 virus was used to generate a standard curve.

Statistical Analysis

All data are shown as mean ± standard deviation (SD). Statistical analysis of data in Fig. 2i,j, and Fig.3h was done using the Mann-Whitney test. Statistical analysis of Fig. 3g was done using Wilcoxon matched-pairs signed rank test. For the other data, statistical analysis was done using paired or unpaired two-tailed Student's t test. $P < 0.05$ was considered to show significantly differences, *p<0.05, **p<0.005, ***p<0.0005.

Data availability

The data that support the findings of this study are available from the corresponding author upon request.

Supplementary Material

Refer to Web version on PubMed Central for supplementary material.

Acknowledgments

This work was supported by NIH AI51354, NIH AI85568, U19AI109962 (N.B), the UC Davis Graduate Group in Immunology, a Vietnamese Education Fellowship to T.T.T.N., a UC Davis Chancellor's Fellowship to N.B. and by the Excellence Initiative of the German Federal and State Governments (EXC 294), by ERC-grant 322972, by the DFG through TRR130 and project 111026 of the German Cancer Aid (M.R). We thank Ms. Spinner (California National Primate Research Center, UC Davis) for help with flow cytometry, Mr. Treister for FlowJo software, Dr. Pohlmeyer for sharing flow cytometry data, and Dr. Cavallari for help with image analysis. We thank Dr. Kubagawa for providing bone marrows from global *Fcmr*$^{-/-}$ mice. Special thanks to the UC Davis Mouse Biology Program for generating the *Fcmr*$^{flx/flx}$*Cd19*-Cre mice.

References

1. Nguyen XH, et al. Toso regulates the balance between apoptotic and nonapoptotic death receptor signaling by facilitating RIP1 ubiquitination. Blood. 2011; 118:598–608. [PubMed: 21613257]
2. Nguyen XH, et al. Antiapoptotic function of Toso (Faim3) in death receptor signaling. Blood. 2012; 119:1790–1791. [PubMed: 22448402]
3. Hitoshi Y, et al. Toso, a cell surface, specific regulator of Fas-induced apoptosis in T cells. Immunity. 1998; 8:461–471. [PubMed: 9586636]
4. Kubagawa H, et al. Identity of the elusive IgM Fc receptor (FcmuR) in humans. The Journal of experimental medicine. 2009; 206:2779–2793. [PubMed: 19858324]
5. Ouchida R, Mori H, Ohno H, Wang JY. FcmuR (Toso/Faim3) is not an inhibitor of Fas-mediated cell death in mouse T and B cells. Blood. 2013; 121:2368–2370. [PubMed: 23520334]
6. Ouchida R, et al. Critical role of the IgM Fc receptor in IgM homeostasis, B-cell survival, and humoral immune responses. Proceedings of the National Academy of Sciences of the United States of America. 2012; 109:E2699–2706. [PubMed: 22988094]
7. Honjo K, et al. Altered Ig levels and antibody responses in mice deficient for the Fc receptor for IgM (FcmuR). Proceedings of the National Academy of Sciences of the United States of America. 2012; 109:15882–15887. [PubMed: 22984178]
8. Choi SC, et al. Mouse IgM Fc receptor, FCMR, promotes B cell development and modulates antigen-driven immune responses. Journal of immunology. 2013; 190:987–996.
9. Lang KS, et al. Involvement of Toso in activation of monocytes, macrophages, and granulocytes. Proceedings of the National Academy of Sciences of the United States of America. 2013; 110:2593–2598. [PubMed: 23359703]

10. Brenner D, et al. Toso controls encephalitogenic immune responses by dendritic cells and regulatory T cells. Proceedings of the National Academy of Sciences of the United States of America. 2014; 111:1060–1065. [PubMed: 24398517]
11. Lang PA, et al. Toso regulates differentiation and activation of inflammatory dendritic cells during persistence-prone virus infection. Cell death and differentiation. 2015; 22:164–173. [PubMed: 25257173]
12. Ouchida R, et al. FcmuR Interacts and Cooperates with the B Cell Receptor To Promote B Cell Survival. Journal of immunology. 2015; 194:3096–3101.
13. Baeuerle PA, Huttner WB. Tyrosine sulfation is a trans-Golgi-specific protein modification. The Journal of cell biology. 1987; 105:2655–2664. [PubMed: 3121635]
14. Lam KP, Kuhn R, Rajewsky K. In vivo ablation of surface immunoglobulin on mature B cells by inducible gene targeting results in rapid cell death. Cell. 1997; 90:1073–1083. [PubMed: 9323135]
15. Niiro H, Clark EA. Regulation of B-cell fate by antigen-receptor signals. Nature reviews Immunology. 2002; 2:945–956.
16. Vire B, David A, Wiestner A. TOSO, the Fcmicro receptor, is highly expressed on chronic lymphocytic leukemia B cells, internalizes upon IgM binding, shuttles to the lysosome, and is downregulated in response to TLR activation. Journal of immunology. 2011; 187:4040–4050.
17. Li FJ, et al. Enhanced levels of both the membrane-bound and soluble forms of IgM Fc receptor (FcmuR) in patients with chronic lymphocytic leukemia. Blood. 2011; 118:4902–4909. [PubMed: 21908424]
18. Shima H, et al. Identification of TOSO/FAIM3 as an Fc receptor for IgM. International immunology. 2010; 22:149–156. [PubMed: 20042454]
19. Thorens B, Schulz MF, Vassalli P. Bone marrow pre-B lymphocytes synthesize immunoglobulin mu chains of membrane type with different properties and intracellular pathways. The EMBO journal. 1985; 4:361–368. [PubMed: 3926483]
20. Nguyen TT, Elsner RA, Baumgarth N. Natural IgM Prevents Autoimmunity by Enforcing B Cell Central Tolerance Induction. Journal of immunology. 2015; 194:1489–1502.
21. Schermelleh L, Heintzmann R, Leonhardt H. A guide to super-resolution fluorescence microscopy. The Journal of cell biology. 2010; 190:165–175. [PubMed: 20643879]
22. Boes M, et al. Enhanced B-1 cell development, but impaired IgG antibody responses in mice deficient in secreted IgM. Journal of immunology. 1998; 160:4776–4787.
23. Sieckmann DG, Stall AM, Subbarao B. A mouse monoclonal antibody specific for an allotypic determinant of the Igha allele of murine IgM: genetic and functional analysis of Igh-6a epitopes using anti-IgM monoclonal antibodies. Hybridoma. 1991; 10:121–135. [PubMed: 1709612]
24. Choi YS, Baumgarth N. Dual role for B-1a cells in immunity to influenza virus infection. The Journal of experimental medicine. 2008; 205:3053–3064. [PubMed: 19075288]
25. Lalor PA, Herzenberg LA, Adams S, Stall AM. Feedback regulation of murine Ly-1 B cell development. European journal of immunology. 1989; 19:507–513. [PubMed: 2785046]
26. Andersson J, Lafleur L, Melchers. IgM in bone marrow-derived lymphocytes. Synthesis, surface deposition, turnover and carbohydrate composition in unstimulated mouse B cells. European journal of immunology. 1974; 4:170–180. [PubMed: 4604559]
27. Klasener K, Maity PC, Hobeika E, Yang J, Reth M. B cell activation involves nanoscale receptor reorganizations and inside-out signaling by Syk. eLife. 2014; 3:e02069. [PubMed: 24963139]
28. Yang J, Reth M. Drosophila S2 Schneider cells: a useful tool for rebuilding and redesigning approaches in synthetic biology. Methods in molecular biology. 2012; 813:331–341. [PubMed: 22083752]
29. Srinivasan L, et al. PI3 kinase signals BCR-dependent mature B cell survival. Cell. 2009; 139:573–586. [PubMed: 19879843]
30. Werner M, Hobeika E, Jumaa H. Role of PI3K in the generation and survival of B cells. Immunological reviews. 2010; 237:55–71. [PubMed: 20727029]
31. Coqueret O. New roles for p21 and p27 cell-cycle inhibitors: a function for each cell compartment? Trends in cell biology. 2003; 13:65–70. [PubMed: 12559756]

32. Gogada R, et al. Bim, a proapoptotic protein, up-regulated via transcription factor E2F1-dependent mechanism, functions as a prosurvival molecule in cancer. The Journal of biological chemistry. 2013; 288:368–381. [PubMed: 23152504]
33. Liu P, Cheng H, Roberts TM, Zhao JJ. Targeting the phosphoinositide 3-kinase pathway in cancer. Nature reviews Drug discovery. 2009; 8:627–644. [PubMed: 19644473]
34. Hayakawa K, et al. Positive selection of natural autoreactive B cells. Science. 1999; 285:113–116. [PubMed: 10390361]
35. Berland R, Wortis HH. Origins and functions of B-1 cells with notes on the role of CD5. Annual review of immunology. 2002; 20:253–300.
36. Baumgarth N, et al. B-1 and B-2 cell-derived immunoglobulin M antibodies are nonredundant components of the protective response to influenza virus infection. The Journal of experimental medicine. 2000; 192:271–280. [PubMed: 10899913]
37. Ochsenbein AF, et al. Control of early viral and bacterial distribution and disease by natural antibodies. Science. 1999; 286:2156–2159. [PubMed: 10591647]
38. Pillai S, Cariappa A. The follicular versus marginal zone B lymphocyte cell fate decision. Nature reviews Immunology. 2009; 9:767–777.
39. Boes M, et al. Accelerated development of IgG autoantibodies and autoimmune disease in the absence of secreted IgM. Proceedings of the National Academy of Sciences of the United States of America. 2000; 97:1184–1189. [PubMed: 10655505]
40. Jackson SW, et al. B cell IFN-gamma receptor signaling promotes autoimmune germinal centers via cell-intrinsic induction of BCL-6. The Journal of experimental medicine. 2016; 213:733–750. [PubMed: 27069113]
41. Rahman MJ, et al. Despite Increased Type 1 IFN, Autoimmune Nonobese Diabetic Mice Display Impaired Dendritic Cell Response to CpG and Decreased Nuclear Localization of IFN-Activated STAT1. Journal of immunology. 2016; 196:2031–2040.
42. Ubelhart R, et al. Responsiveness of B cells is regulated by the hinge region of IgD. Nature immunology. 2015; 16:534–543. [PubMed: 25848865]
43. Fuchs EJ, Matzinger P. B cells turn off virgin but not memory T cells. Science. 1992; 258:1156–1159. [PubMed: 1439825]
44. Baumgarth N, et al. Innate and acquired humoral immunities to influenza virus are mediated by distinct arms of the immune system. Proceedings of the National Academy of Sciences of the United States of America. 1999; 96:2250–2255. [PubMed: 10051627]
45. Stall AM, Wells SM, Lam KP. B-1 cells: unique origins and functions. Seminars in immunology. 1996; 8:45–59. [PubMed: 8850298]
46. Choi YS, Dieter JA, Rothaeusler K, Luo Z, Baumgarth N. B-1 cells in the bone marrow are a significant source of natural IgM. European journal of immunology. 2012; 42:120–129. [PubMed: 22009734]
47. Doucett VP, et al. Enumeration and characterization of virus-specific B cells by multicolor flow cytometry. J Immunol Methods. 2005; 303:40–52. [PubMed: 16045923]
48. Snapp EL, Altan N, Lippincott-Schwartz J. Measuring protein mobility by photobleaching GFP chimeras in living cells. Current protocols in cell biology/editorial board, Juan S. Bonifacino ... [et al.]. 2003; Chapter 21(Unit 21):21.
49. Feder TJ, Brust-Mascher I, Slattery JP, Baird B, Webb WW. Constrained diffusion or immobile fraction on cell surfaces: a new interpretation. Biophysical journal. 1996; 70:2767–2773. [PubMed: 8744314]
50. Lippincott-Schwartz J, et al. Monitoring the dynamics and mobility of membrane proteins tagged with green fluorescent protein. Methods in cell biology. 1999; 58:261–281. [PubMed: 9891386]
51. Reimold AM, et al. Plasma cell differentiation requires the transcription factor XBP-1. Nature. 2001; 412:300–307. [PubMed: 11460154]

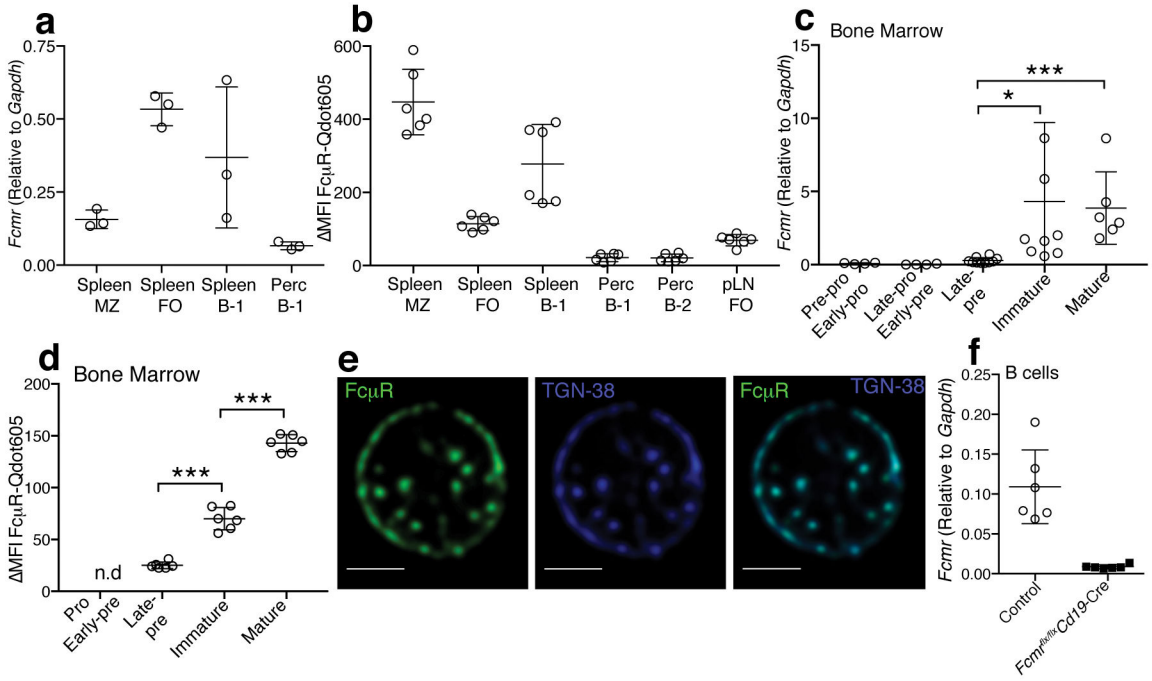

Figure 1. The FcμR is expressed by various cell subsets

(**a**) *Fcmr* mRNA expressions in different B cell subsets in spleen and peritoneal cavities (perc): marginal zone (MZ), follicular (FO), spleen B-1, and perc B-1 cells. Each symbol represents values from one mouse (n=3 mice). (**b**) Surface FcμR expression in different B cell subsets in spleen, perc, and inguinal lymph node (pLN) (n=6 mice) (**c**) *Fcmr* mRNA expression by different B cell developmental stages (n = 4–10 samples/group, each sample was sorted from BM of 2 mice). (**d**) Surface FcμR expression by pro- and early pre- B cells, late pre-, immature and mature B cells (n=6 mice). (**e**) Confocal microscopy of immature B cells stained with FcμR (green) and TGN-38 (blue). White bars indicate 2 μm scale bars. (**f**) Relative expression of *Fcmr* mRNA of purified *Fcmr* $^{flx/flx}$*Cd19*-Cre and control B cells (n=6 mice/group). Data are combined from 3 independent experiments (**c**) or are representative of at least two independent experiments (**a–b**, **d–f**) (mean ± SD in **a–d, f**). *p<0.05, **p<0.005, ***p<0.0005 by unpaired two-tailed Student's *t*-test.

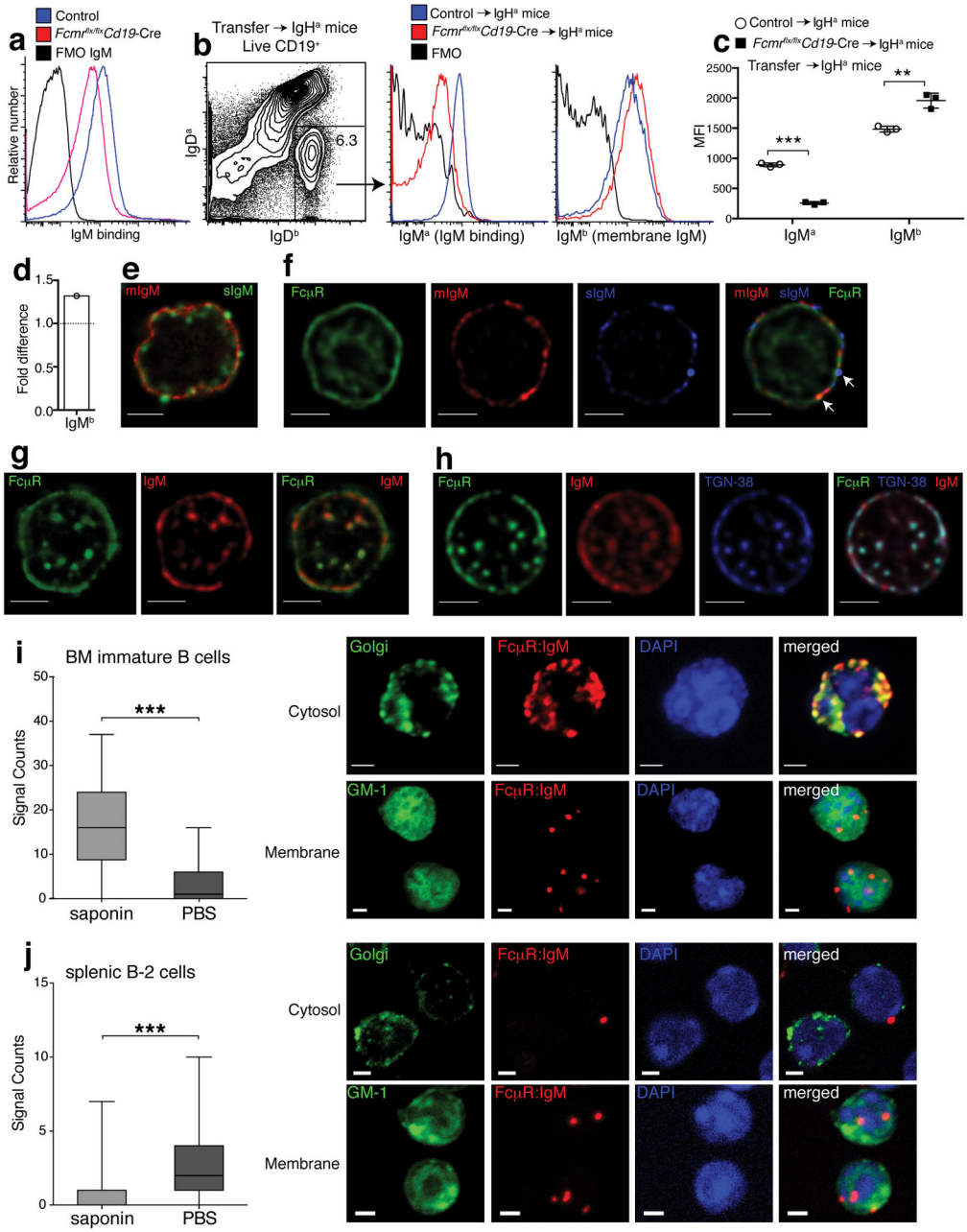

Figure 2. IgM FcμR interaction occurs with both secreted and membrane IgM

(**a**) Shown are histogram plots of splenic B cells from control and *Fcmr* $^{flx/flx}$*Cd19*-Cre mice incubated or not with biotinylated IgM and stained with streptavidin-PE. (**b**) Splenocytes from *Fcmr* $^{flx/flx}$*Cd19*-Cre and control mice (IgH^{b}) were i.v transferred into C6.IgH^{a} mice (n=3 mice/group). Shown are 5% contour plots with outliers gated on live CD19^{+} B cells, identifying transferred B cells as IgD^{a-} and IgD^{b+}. (**c**) Overlay histograms comparing IgM^{a} (in vivo sIgM binding) and IgM^{b} (membrane IgM) expression of transferred B cells (IgD^{a-} IgD^{b+}) from *Fcmr* $^{flx/flx}$*Cd19*-Cre and control mice 3 days after transfer. Graph summarizes mean fluorescence intensities ± SD of IgM^{a} and IgM^{b} staining of transferred B cells. (**d**)

Fold-difference in MFI from IgM^b (mIgM) of *Fcmr*$^{flx/flx}$*Cd19*-Cre B cells compared to controls. (**e,f**) Follicular B cells unable to secrete IgM ($\mu_s^{-/-}$) were isolated from mixed BM $\mu_s^{-/-}$ (IgM^a) and WT (IgM^b) chimeras. (**e**) STED microscopy of $\mu_s^{-/-}$ B cells stained for sIgM (IgM^b-green) and mIgM (IgM^a-red). (**f**) Confocal microscopy of $\mu_s^{-/-}$ follicular B cells stained for FcμR (green), mIgM (IgM^a, red), and sIgM (IgM^b, blue). White arrows identify co-localization of FcμR with mIgM or sIgM. (**g**) STED microscopy of immature B cells stained for FcμR (green) and IgM (red). (**h**) Confocal microscopy of immature B cells stained with FcμR (green), IgM (red) and TGN-38 (blue). Scale bars 2μm. (**i–j**) Quantified box-and-whisker-plots (min, max, median, quartiles) and microscopic representation of Proximal ligation assay (PLA) of GFP-sorted (**i**) BM immature (n=250 cells) and (**j**) splenic mature B cells (n=750 cells) treated with or without saponin prior to PLA, as indicated. Red indicates FcμR-IgM interaction. Green shows staining of Golgi network using labeled lectin-GSII staining (J-top, K-top) or GM-1 staining indicating the cell membrane, using labeled cholera-toxin subunit B (J-bottom, K-bottom). DAPI stained nuclei presented in blue. Scale bar 2μm. Data are representative of at least two independent experiments. *$p<0.05$, **$p<0.005$, ***$p<0.0005$ by unpaired two-tailed Student's *t*-test (**a–c**) or Mann-Whitney test (**i–j**).

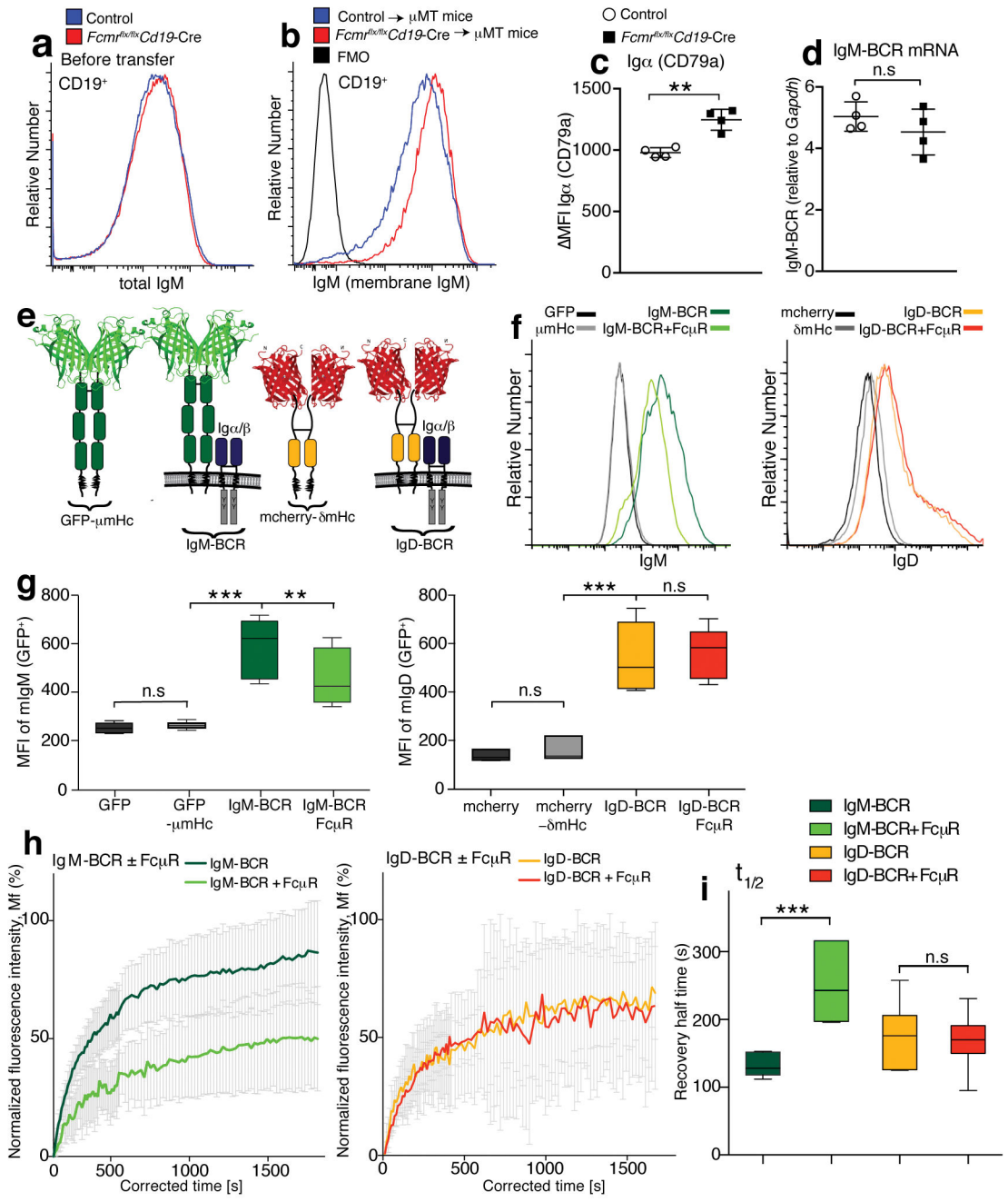

Figure 3. FcμR-mIgM interactions constrain BCR surface expression

(**a**) Overlay histogram flow cytometry plots comparing total surface IgM staining (membrane plus secreted IgM binding), on splenic CD19^{+} B cells from *Fcmr*$^{flx/flx}$*Cd19*-Cre and control mice. (**b**) Overlay histograms comparing IgM (membrane IgM) expression on B cells (IgD^{a-} IgD^{b+}) from *Fcmr*$^{flx/flx}$*Cd19*-Cre and control mice 3 days after transfer into IgH^{a} mice. (**c**) Mean fluorescence intensities ± SD of staining for Igα (CD79a) in total spleen B cells from *Fcmr*$^{flx/flx}$*Cd19*-Cre and control mice (n=4 mice/group). (**d**) Mean relative expression of membrane IgM (BCR) mRNA ± SD of purified *Fcmr*$^{flx/flx}$*Cd19*-Cre and control B cells (n=4 mice/group). Data are representative of at least two independent

experiments. (**e**) Model of the GFP-μm heavy chain (GFP-μmHc) and the assembled chimeric IgM-BCR containing the CD79a and CD79b signaling subunits, the mcherry-δmHc and the assembled chimeric IgD-BCR expressed in S2 cells. (**f**) Shown are flow cytometry histogram plots of Drosophila S2 cells stained for IgM or IgD. The cells expressed GFP, GFP-μmHc, mcherry-δmHc, IgM-BCR ± FcμR, IgD-BCR ± FcμR. (**g**) Box-and-whisker-plots (min, max, median, quartiles) summarize MFI of surface IgM (left) and surface IgD (right) expression by S2 cells after transfection. (**h,i**) Shown are IgM (left) and IgD (right) re-expression by transfected S2 cells after photobleaching (FRAP) (n=50 cells). The cells expressed the IgM-BCR as GFP-coupled chimera described in (**e**) and the IgD-BCR GFP-chimera with or without the FcμR. (**h**) Mean ratios of fluorescence staining of the mobile fraction (Mf) ± SD. (**i**) Box-and-whisker-plots (min, max, median, quartiles) summarize the half-time recovery. Data are representative of at least two independent experiments (**a–d, h–i**). Data are combined from five independent experiments (**f–g**). n.s. not significantly different, *p<0.05, **p<0.005, ***p<0.0005 by unpaired two-tailed Student's *t*-test (**c,d,i**), Wilcoxon matched-pairs signed rank test (**g**), or Mann-Whitney test (**h,** ***p<0.0001 for IgM-BCR, and n.s for IgD-BCR).

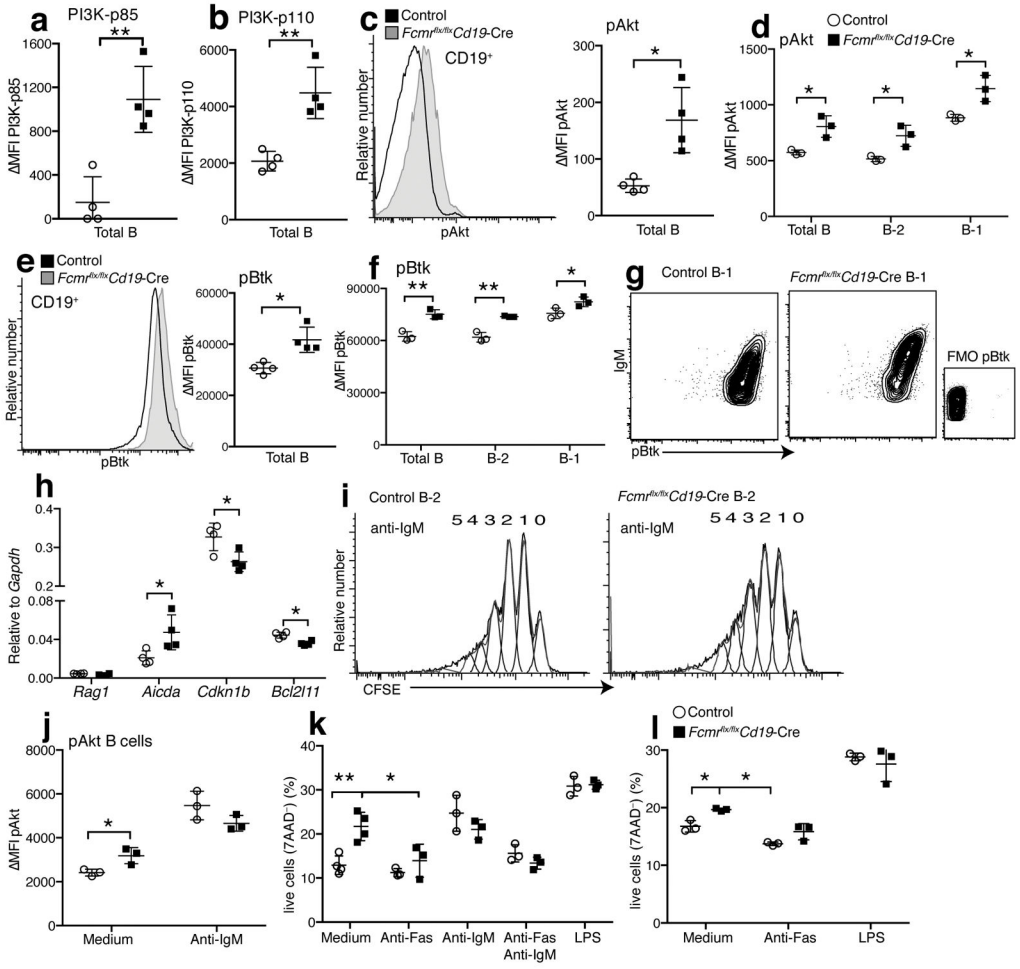

Figure 4. Enhanced tonic BCR signaling in *Fcmr*$^{-/-}$ B cells

(**a–c**) MFI ± SD of *ex vivo* staining for expression of (**a**) PI3K-p85 and (**b**) PI3K-p110 by flow cytometry. (**c**) Overlay histograms (left) and graph summarizing MFI ± SD of phospho (p)Akt expression by total B cells from *Fcmr*$^{flx/flx}$*Cd19*-Cre mice and *Fcmr*$^{flx/flx}$ Cre-negative controls (right). (**d**) pAkt expression levels in total spleen B cells, FO B (B-2) and B-1 cells. (**e**) Overlay histograms of phospho (p)Btk expression by total B cells from indicated mice (left). Graph summarizing MFI ± SD of phospho (p)Btk expression. (**f**) pBtk expression in total spleen B cells, FO B (B-2) and B-1 cells from *Fcmr*$^{flx/flx}$*Cd19*-Cre and control mice (n=3–4 mice/group). (**g**) 5% contour plots with outliers gated on lived splenic B-1 cells from *Fcmr*$^{flx/flx}$*Cd19*-Cre and control mice, showing the correlation of surface IgM and pAkt expression. (**h**) mRNA expression levels of FOXO target genes *Rag1*, *Aicda*, *Cdkn1b*, and *Bcl2l11* in *Fcmr*$^{flx/flx}$*Cd19*-Cre and control B cells after normalization to *Gapdh* (n=4 mice/group). (**i**) FO B cells isolated from spleens of *Fcmr*$^{flx/flx}$*Cd19*-Cre and control mice labeled with CFSE and stimulated with anti-IgM for 72h. Numbers are rounds of cell divisions. (**j**) pAkt expression levels (ΔMFI= mean fluorescent intensity (MFI) – MFI fluorescence minus one (FMO) control) after 72h culture with/without anti-IgM. (**k**) FO B-2 cells isolated from *Fcmr*$^{flx/flx}$*Cd19*-Cre and control spleens stimulated as indicated for 72h. Frequencies of live cells as determined by 7-AAD staining. (**l**) Frequencies of live (7-AAD^{-})

B-1 cells isolated from *Fcmr*$^{flx/flx}$*Cd19*-Cre and control spleens and stimulated as indicated for 48h (n=3 samples pooled from 2 mice (**k–l**)). Each data set is representative of at least two independent experiments (mean ± SD in **a–f, h, j–l**). *p<0.05, **p<0.005 by unpaired two-tailed Student's *t*-test.

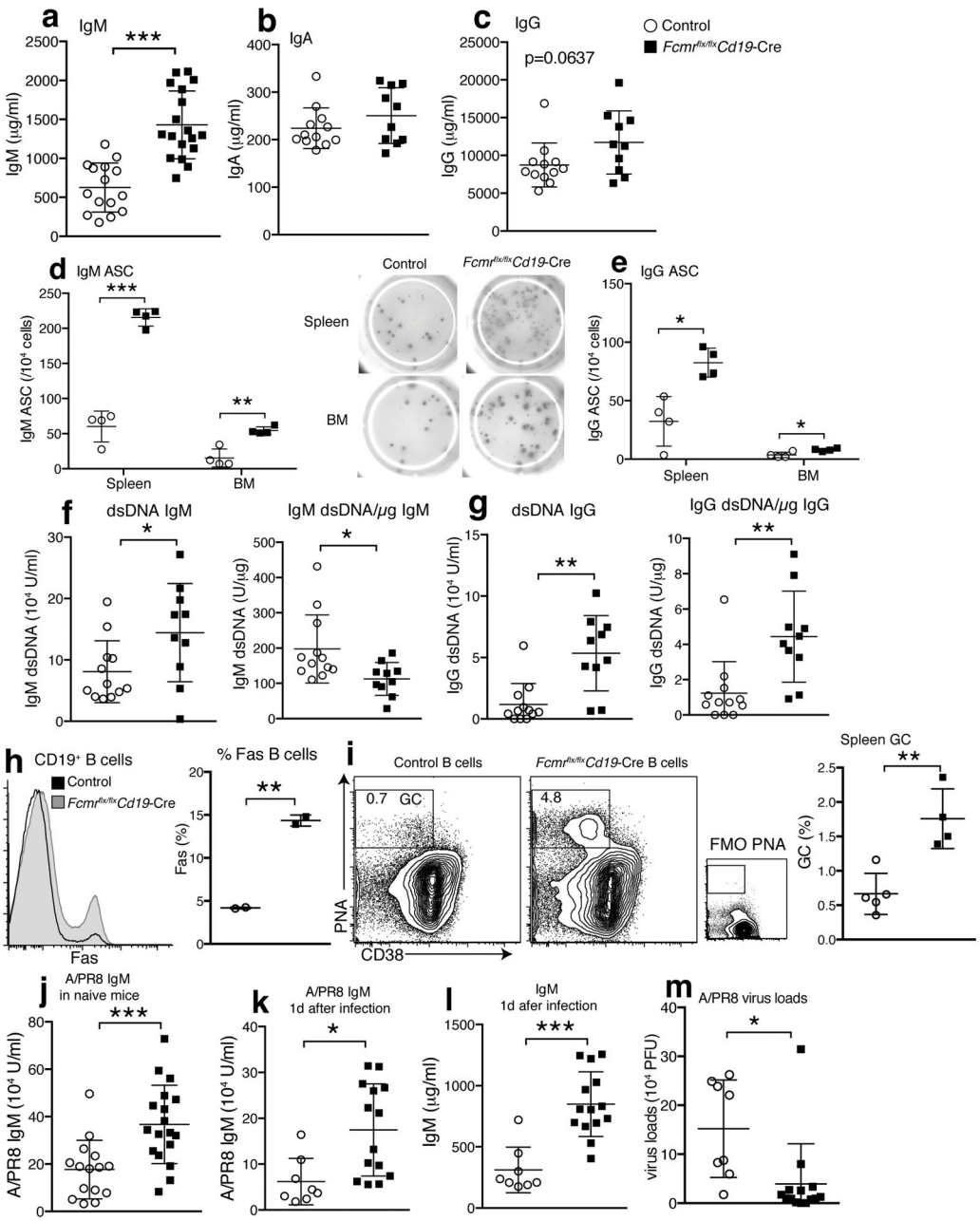

Figure 5. Increased influenza-protective natural IgM and autoantibody production in *Fcmr*$^{flx/flx}$*Cd19*-Cre mice

Concentrations of (**a**) IgM, (**b**) IgA, (**c**) IgG in *Fcmr*$^{flx/flx}$*Cd19*-Cre and control sera from 3 months old mice (n=10–18 mice/group). (**d**) Frequencies of IgM and (**e**) IgG secreting cells in spleens and BMs of these mice (n=4 mice/group). (**f**) Relative amounts of IgM and (**g**) IgG anti-dsDNA and relative amounts of anti-dsDNA/mg Ig per μg total Ig in *Fcmr*$^{flx/flx}$*Cd19*-Cre and control sera (n=10–12 mice/group). (**h**) Overlay histograms of Fas expression by B cells from indicated mice (left). Graph summarizing results (right) (n=2 mice/group). (**i**) 5% contour plots with outliners gated on live CD19^{+} B cells. Gate and numbers identify CD38^{low} PNA^{+} germinal center (GC) B cells. Graphs summarize

frequencies ± SD GC B cells of total cells in *Fcmr*$^{flx/flx}$*Cd19*-Cre and control spleens (n=4–5 mice/group). (**j**) Relative amounts influenza A/Puerto Rico/8/34-binding IgM in sera from naïve *Fcmr*$^{flx/flx}$*Cd19*-Cre and control mice (n=15–18 mice/group). (**k**) Relative amounts of influenza A/PR8-binding and (**l**) total IgM in sera of *Fcmr*$^{flx/flx}$*Cd19*-Cre, and control mice one day after A/PR8 infection (n=8, 14 mice/group). Data are representative of at least two independent experiments. (**m**) Lung viral loads at 1 day after A/PR8 infection. For Figure **k**, **l** and **m** data are combined from three independent experiments (mean ± SD in **a–m)**. *p<0.05, **p<0.005, ***p<0.0005 by unpaired two-tailed Student's *t*-test.

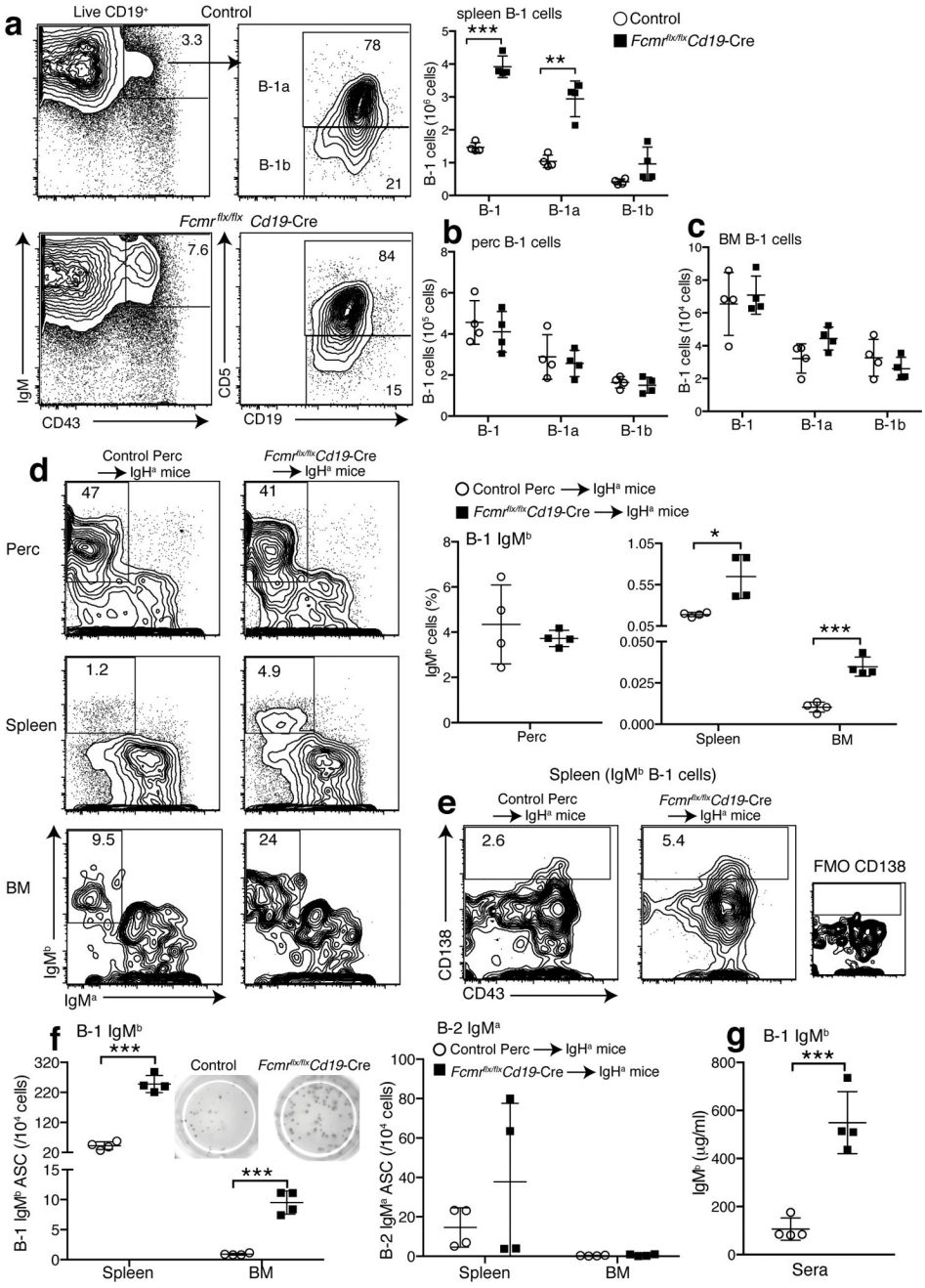

Figure 6. B-1 cells are responsible for increased natural IgM secretion in *Fcmr* $^{flx/flx}$*Cd19*-Cre mice

(**a**) 5% contour plots with outliers gated for live CD19^{+} spleen B cells from control and *Fcmr* $^{flx/flx}$*Cd19*-Cre mice. B-1 cells were identified as: CD43^{+} IgM^{hi} CD19^{hi} and CD5$^{+/-}$ (B-1a/B-1b). Graph summarizes numbers of B-1 cells, including B-1a and B-1b cells in spleen, (**b**) peritoneal cavity and (**c**) BM (n=4 mice/group). (**d–g**) Generation of chimeras with *Fcmr*$^{-/-}$ B-1 (IgH^{b}) and wild-type B-2 (IgH^{a}) cells and controls (n=4 mice/group). (**d**) (left) 5% contour plots with outliers gated for lived CD19^{+} B cells from peritoneal cavities and spleens. For BM, cells were pre-gated for B-1 cells (CD19^{+} IgM^{+} CD43^{+}). The

transferred B-1 cells were identified as IgM^{b+} IgM^{a-}. Graph provides summary of IgM^{b} B-1 cell frequencies in indicated tissues. (**e**) 5% contour plots with outliers gated on IgM^{b+} B-1 cells in spleen. Gates and numbers identify frequencies of $CD138^{+}$ of IgM^{b+} B-1 cells. FMO, fluorescence minus one control. (**f**) Graphs summarize the frequencies of IgM^{b} secreting B-1 (left) and IgM^{a} secreting B-2 cells (right) in spleen, and BMs. (**g**) Serum IgM^{b} levels in the chimera. Data are representative of at least two independent experiments (**a–c**) (mean ± SD in **a–d, f–g**). *p<0.05, **p<0.005, ***p<0.0005 by unpaired two-tailed Student's t-test.

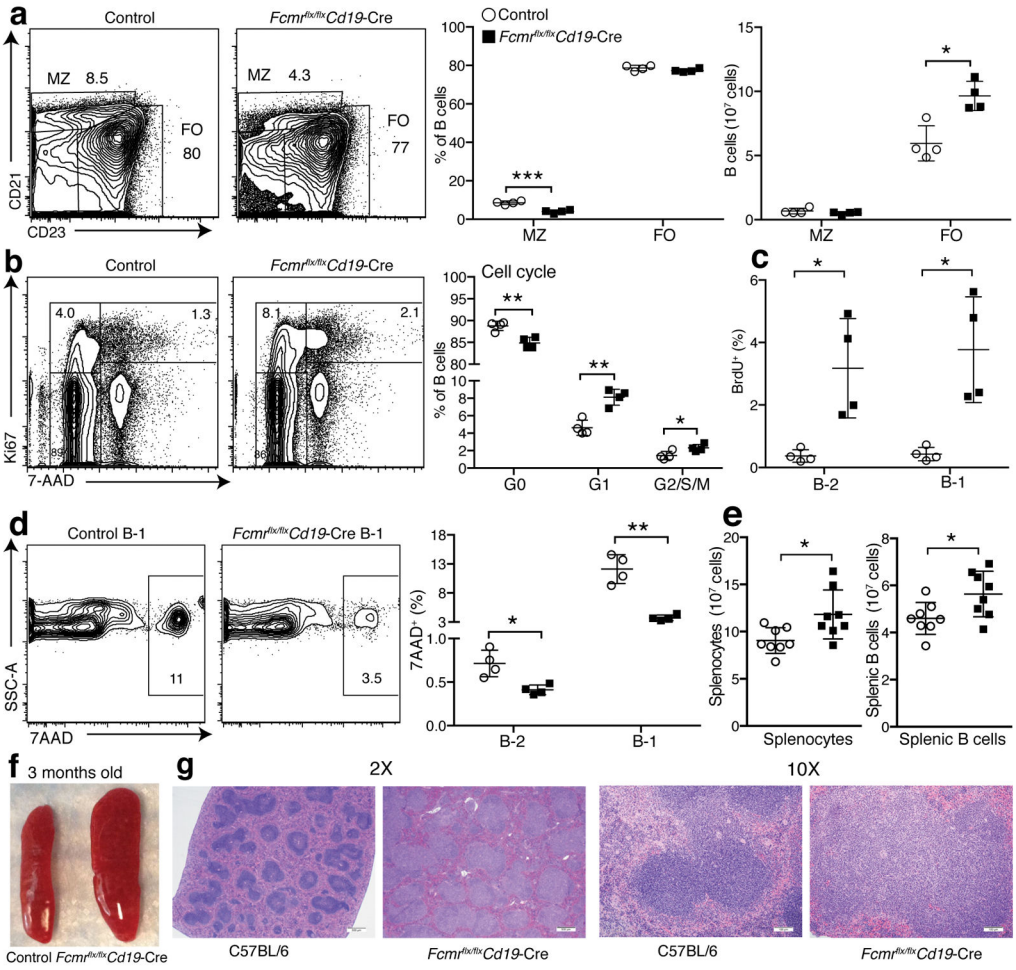

Figure 7. Increased B cell turnover and cell survival of B cells result in B cell lymphocytosis

(**a**) 5% contour plots with outliers of representative spleen samples (n=4 mice/group) from *Fcmr* $^{flx/flx}$*Cd19*-Cre and control mice analyzed by flow cytometry after gating on live CD19^{+} B cells. Identified subsets: CD21^{hi}CD23^{-} marginal zone B cells (MZ); CD21^{int}CD23^{+} follicular B cells (FO) (left). Graph summarizes frequencies (middle) and numbers (right) of MZ and FO in *Fcmr* $^{flx/flx}$*Cd19*-Cre and control spleens. (**b–c**) Cell cycle/turnover analysis of CD19^{+} live spleen B cells from *Fcmr* $^{flx/flx}$*Cd19*-Cre and control mice (n=4 mice/group). (**b**) 5% contour plots with outliers of live CD19^{+} B cells from indicated mice, identifying cell cycle stages by Ki67 and 7-AAD staining (G0: Ki67^{-} 7AAD^{-}, G1: Ki67^{+} 7AAD^{-}; G2/S/M: Ki67^{+} 7AAD^{+}). Graph summarizes frequencies (n = 4 mice/group). (**c**) B-2 and B-1 cell turnover was determined by flow cytometry 24h after i.p. injection of BrdU. Shown are frequencies of BrdU^{+} cells (n=4 mice/group). (**d**) 5% contour plots with outliers gated on 7AAD^{+} (dead cells) among splenic live CD19^{+} CD43^{+} IgM^{hi} IgD^{lo} B-1 cells (left). Shown are frequencies of 7AAD^{+} cells (n=4 mice/group; right). (**e**) Total spleen (left) and B cell counts (right) of indicated mice (n=8 mice/group). (**f**) Photo of representative spleens from 3-months old control and *Fcmr* $^{flx/flx}$*Cd19*-Cre mice. (**g**) H&E staining of spleens from 8-months old C57BL/6 and *Fcmr* $^{flx/flx}$*Cd19*-Cre mice. 2X scale bar is 500μm, 10X scale bar is 100μm. Data are representative of at least two independent

experiments. Data are combined from two independent experiments (**f**) (mean ± SD in **a–e**). *p<0.05, **p<0.005, ***p<0.0005 by unpaired two-tailed Student's t-test.